



Delft University of Technology

Parametric Study of a Switchable Vortex Generator for Load Alleviation in Transonic Conditions

Marino, Luca; Kiat, Ilias; Eberle, Adrian; Sodja, Jurij

DOI

[10.2514/1.C037939](https://doi.org/10.2514/1.C037939)

Publication date

2025

Document Version

Final published version

Published in

Journal of Aircraft

Citation (APA)

Marino, L., Kiat, I., Eberle, A., & Sodja, J. (2025). Parametric Study of a Switchable Vortex Generator for Load Alleviation in Transonic Conditions. *Journal of Aircraft*, 62(3), 579-593.
<https://doi.org/10.2514/1.C037939>

Important note

To cite this publication, please use the final published version (if applicable).
Please check the document version above.

Copyright

Other than for strictly personal use, it is not permitted to download, forward or distribute the text or part of it, without the consent of the author(s) and/or copyright holder(s), unless the work is under an open content license such as Creative Commons.

Takedown policy

Please contact us and provide details if you believe this document breaches copyrights.
We will remove access to the work immediately and investigate your claim.

**Green Open Access added to [TU Delft Institutional Repository](#)
as part of the Taverne amendment.**

More information about this copyright law amendment
can be found at <https://www.openaccess.nl>.

Otherwise as indicated in the copyright section:
the publisher is the copyright holder of this work and the
author uses the Dutch legislation to make this work public.

Parametric Study of a Switchable Vortex Generator for Load Alleviation in Transonic Conditions

Luca Marino* and Ilias Kiat†

Delft University of Technology, 2629 HS Delft, The Netherlands

Adrian Eberle‡

Airbus Operations, GmbH, 28199 Bremen, Germany

and

Jurij Sodja§

Delft University of Technology, 2629 HS Delft, The Netherlands

<https://doi.org/10.2514/1.C037939>

This paper investigates the impact of introducing a switchable vortex generator (SVG), acting as a minitab, on the aerodynamic performance of a high-aspect-ratio wing's outer section in transonic regime. A parametric study is conducted employing computational fluid dynamics two-dimensional simulations, focusing on the aerodynamic effects of changing the chordwise position and height of the vane of a SVG located on the airfoil upper surface in both nominal cruise conditions and for varying angles of attack. The analysis reveals that minitabs can strongly affect the aerodynamic forces produced by the wing section, showing great potential for load alleviation and control, but also emphasizing the need for a careful parameter selection to reduce undesirable effects such as the generation of shock waves. In cruise conditions, lift reduction increases with the vane height and has its maximum for chordwise positions at 60% of the chord length. However, SVGs located in the first half of the chord length yield more robust performance for varying angle of attack, without sharp lift variations or generated shock waves, and a delayed stall onset. High SVGs (greater than or equal to 3% chord length) can also lead to strong shock waves on the airfoil lower surface at small or negative angle of attack, while small SVGs (less than 1% chord length) can generate normal shock waves on the upper surface, with limited lift reduction in cruise conditions and at higher incidence.

Nomenclature

b	=	wingspan
C_d	=	drag coefficient
C_{fx}	=	skin friction coefficient
C_l	=	lift coefficient
C_p	=	pressure coefficient
c	=	chord length
h	=	height of the vortex generator vane
M	=	Mach number
Re	=	Reynolds number
U	=	flow velocity magnitude
x	=	coordinate along the chordwise direction
x^*	=	vortex generator position along the chord line
y	=	coordinate along the wing span
y^+	=	dimensionless wall distance parameter
z	=	coordinate normal to the chordwise direction in the airfoil plane
α	=	angle of attack
γ	=	heat capacity ratio
Λ	=	sweep angle

I. Introduction

AIRCRAFT encounter a wide range of aerodynamic loads during their operation, including those induced by gusts, atmospheric turbulence, and maneuvers. These loads can exert considerable stress on structural elements, potentially leading to fatigue, excessive deformation, or even catastrophic failure. Load alleviation and control strategies are developed to address these challenges by mitigating the magnitude and fluctuations of the aerodynamic loads. By effectively reducing the loads acting on the aircraft's structure, these techniques enhance fatigue life, reduce weight requirements, and improve overall structural reliability [1].

Passive load alleviation strategies involve the use of fixed devices, such as stall triggers applied to wing's leading edge, or modifications to the aircraft's structure to passively reduce aerodynamic loads by inducing wash-out and/or controlling airflow separation. However, the effectiveness of these techniques is limited to specific flight conditions and may not provide significant load alleviation in all scenarios or adapt to changing aerodynamic conditions. Active load alleviation and control are often achieved by employing control surfaces, such as flaps, ailerons, spoilers, and wing morphing mechanisms, and allow the management and redistribution of aerodynamic loads in response to changing conditions [2,3]. Nonetheless, the large inertia of the control surfaces limits their efficacy in controlling loads characterized by high reduced frequencies [4]. Although more and more advanced actuators have been developed in recent years to achieve faster time response and higher performance in terms of stroke and bandwidth (see, e.g., Ref. [5]), active load control systems generally require advanced sensors and control algorithms, adding weight and complexity to the aircraft, along with the need for a careful design to avoid undesirable dynamic interactions [6].

In recent years, different studies have investigated the potential of using small mechanical devices, called minitabs, to impact the lift provided by the airfoil. This concept can be seen as a generalization of the Gurney flap's principle. Gurney flaps are thin tabs perpendicular to the airflow. In aeronautical applications, they are typically installed on the lower surface of an airfoil, near the trailing edge, to provide lift increase. When air flows over the airfoil, the Gurney flap produces a separated region characterized by a counterrotating vortex pair

Presented as Paper 2024-2110 at the AIAA SciTech 2024 Forum, Orlando, FL, January 8–12, 2024; received 14 February 2024; accepted for publication 18 October 2024; published online 16 January 2025. Copyright © 2025 by Luca Marino, Ilias Kiat, Adrian Eberle, and Jurij Sodja. Published by the American Institute of Aeronautics and Astronautics, Inc., with permission. All requests for copying and permission to reprint should be submitted to CCC at www.copyright.com; employ the eISSN 1533-3868 to initiate your request. See also AIAA Rights and Permissions www.aiaa.org/randp.

*Research Associate, Faculty of Aerospace Engineering, Department of Aerospace Structures and Materials, Kluyverweg 1; l.marino-1@tudelft.nl.

†M.Sc. Student, Faculty of Aerospace Engineering, Department of Aerospace Structures and Materials, Kluyverweg 1; i.kiat@student.tudelft.nl.

‡R&T Project Leader, Flight Physics, Technology Strategy & Integration, Airbus-Allee 1; adrian.eberle@airbus.com.

§Assistant Professor, Faculty of Aerospace Engineering, Department of Aerospace Structures and Materials, Kluyverweg 1; j.sodja@tudelft.nl.

behind the flap, displacing the Kutta condition downstream and increasing the suction peak on the upper surface [7–10], hence increasing the overall airfoil lift. The use of similar minitabs mounted on the upper surface, physically acting as minispoilers, has also proved effective for lift reduction purposes [11,12]. Further studies explored the effects of placing minitabs/spoilers at different chordwise locations. Compared to the placement at the trailing edge, moving the minitabs upstream up to $x_f/c > 0.70$ was shown to reduce the lift decrease at $\alpha = 0^\circ$ [13,14]. On the other hand, the employment of minitabs in proximity of the leading edge has yielded small advantages at low angles of attack (AOA) but provides a significant lift decrease for higher incidence. Finally, locations around $x_f/c = 0.60$ appear to offer an effective lift reduction for a wide range of AOA [4,15,16]. Two-dimensional [17] and three-dimensional [18] experimental studies were also conducted to evaluate the effectiveness of minitabs and spoilers for lift reduction in the presence of unsteady wing motion, showing that load alleviation can still be achieved if unsteady effects of limited magnitude occur. Nonetheless, while numerical and experimental results presented in these contributions show that the use of mechanical devices such as minitabs has great potential for load alleviation purposes, it is also clear that their performance is strongly dependent on geometrical factors such as their height, orientation, and chordwise location. This suggests that even better performances could be achieved by using minitabs designed to be activated or rotated in response to changing aerodynamic conditions. However, further research is needed to fully assess the impact of these design factors on the aerodynamic load alleviation. Moreover, most studies are currently limited to subsonic conditions, thus offering a limited insight on the potential effects of using minitabs in transonic conditions, where transonic aerodynamic effects could reduce their performance.

Although the use of minitabs has mostly been explored for purposes such as controlling aerodynamic loads in high-speed and low-AOA conditions, small triangular-shaped fins or plates known as vortex generators (VGs) are usually mounted on aircraft's surfaces to augment their aerodynamic performance during low-speed and high-AOA flight regimes. Through the generation of vortices that are shed downstream, VGs aim at reenergizing the turbulent boundary layer, delaying flow separation and reducing the risk of premature stalls [19]. Conventional, passive, vane-type VGs [20], with vane height comparable to the boundary-layer thickness, are currently the preferred option for flow separation control [21], mostly because of their design simplicity, ease of manufacture, installation, and low maintenance [22]. Several research studies [21,23–26] have been conducted to determine the effectiveness of these VGs for varying height, orientation, shape, and location. In particular, it was found that good performances in lift generation can also be achieved by employing VGs whose height is only a fraction of the boundary-layer thickness, avoiding the significant residual drag increase caused by conventional VGs [19,21]. Finally, the use of active smart vortex generators, actuated using shape memory alloys, has also been investigated in recent years [27–30]. These VGs showed an improved capability of increasing lift and

stall angle, while inducing a negligible rise in drag in nominal cruise conditions. However, while the working principles of traditional, passive VGs are generally well understood, further investigations are still needed to determine whether active VGs can operate reliably in a broad range of aircraft operating conditions and how their design parameters can be selected to meet this requirement in different aerodynamic conditions.

Switchable vortex generators (SVGs) are among those novel concepts which are being developed to improve flow separation control and load alleviation performances in the next generation of wings. In particular, load alleviation and control becomes a key factor in high-aspect-ratio wings, where offloading outer wing sections is vital to avoid the oversizing of the wing structure, and the consequent weight penalty. In these devices, the dual purpose of alleviating aerodynamic loading and preventing stall can simply be achieved by rotating the vortex vane, as shown in Fig. 1:

1) In high-speed, low-AOA conditions, the vane can be rotated perpendicularly to the incoming airflow, hence acting as a spoiler and inducing flow separation.

2) In low-speed, high-AOA conditions, the vane can be rotated at an angle between 0 and 90 deg to delay or suppress flow separation through the generation of streamwise vortices.

The spoiler function of the SVG can be particularly useful to offload wing sections with high structural loads in high-speed off-design conditions, such as maneuvering and in the event of gusts or turbulence, which generally define the critical load cases for structural sizing. Moreover, an important advantage of SVGs is that they can be deployed on demand only when their functionality is required. For the remaining part of the operational time, such VGs can be maintained in an aerodynamically neutral position to allow for optimal aerodynamic performance in terms of drag (Fig. 1, case C).

This paper aims at assessing the load alleviation performance of the spoiler configuration of a SVG operated on a supercritical airfoil, in transonic conditions. To this end, the aerodynamic behavior of an outer section of a new-generation high-aspect-ratio DLR-F25 wing (shown in Fig. 2) is investigated in the presence of a minitab mounted on the airfoil's upper surface. A parametric study is conducted, by means of two-dimensional computational fluid dynamics (CFD) simulations, to determine how the design parameters of the SVG, namely, the height of the vortex vane and the chordwise position, can affect lift and drag generation at transonic speeds. To further elucidate these aerodynamic effects, pressure and skin friction coefficients distributions and the velocity airflow around the airfoil will be examined. Moreover, a sensitivity analysis is conducted to establish how the performance of the spoiler function of the SVG is affected by different angles of attack.

The paper is organized as follows. Section II introduces the analysis methodology. The investigation into the effects from height and chordwise location of the SVG is presented in Sec. III. The sensitivity analysis of the SVG performance with respect to the angle of attack is showcased in Sec. IV. Finally, concluding remarks are summarized in Sec. V.

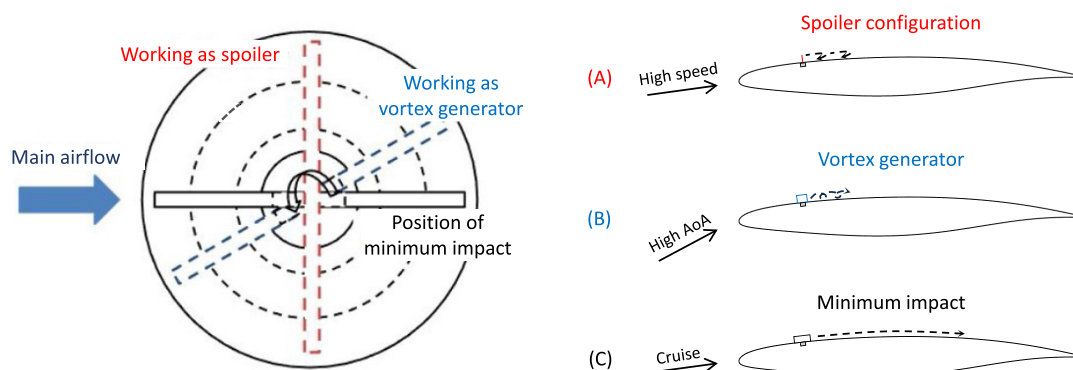


Fig. 1 Concept design of a switchable vortex generator.

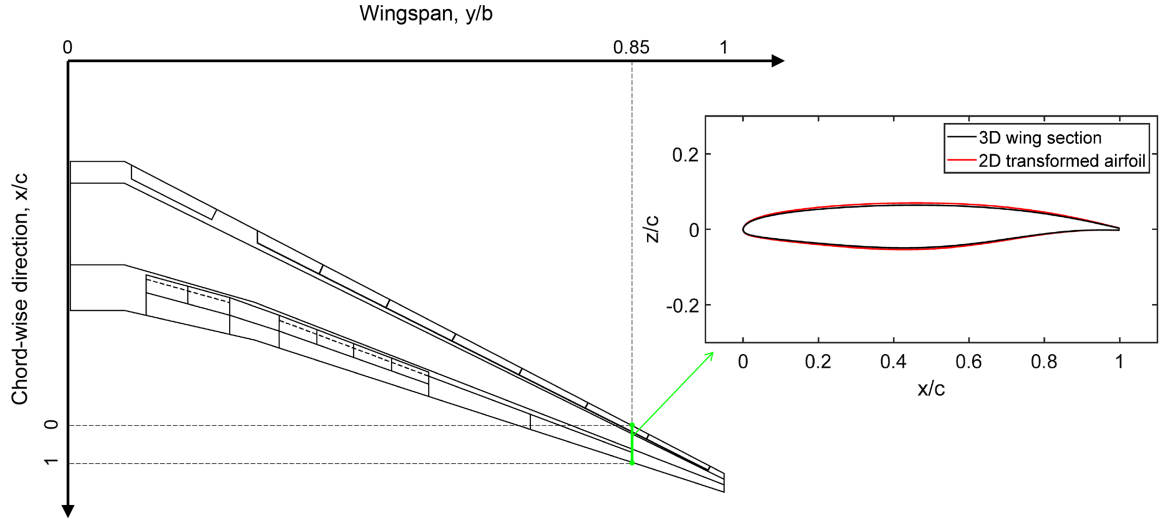


Fig. 2 Layout of the DLR-F25 wing and outer wing section at $y/b = 0.85$ selected for the parametric study.

II. Analysis Methodology

The spoiler configuration of the switchable vortex generator is meant to alleviate the aerodynamic load acting on the outboard portion of the wing in high-speed conditions. In this paper, the effect of the SVG on the aerodynamic performance of a wing section is assessed by conducting two-dimensional (2D) CFD simulations for varying vane heights and chordwise location, considering nominal cruise conditions and high-speed off-design conditions characterized by different values of the angle of attack. Consistently with the scope of the spoiler function of the SVG, an outer section of the DLR-F25 wing, located at $y/b = 0.85$, has been selected as a case study for the investigation, as illustrated in Fig. 2. The properties of the airflow in cruise conditions for the DLR-F25 wing are specified in Table 1.

A. Geometry Transformation for Two-Dimensional Analysis

Because the validity of a two-dimensional analysis is limited to the plane of the aerodynamic field where orthogonal gradients are zero [31], the so-called rule of cosine has been considered in this study to account for the wing sweep effects [32]. In particular, the chord length and coordinates of the airfoil have been transformed as

$$c_{2D} = c_{3D} \cos \Lambda_s \quad x_{2D} = x_{3D} \cos \Lambda_s \quad z_{2D} = z_{3D} \quad (1)$$

generating the geometry illustrated in Fig. 2. Furthermore, the velocity of the airflow has been scaled as

$$V_{\infty,2D} = V_{\infty,3D} \cos \Lambda_s \quad (2)$$

to represent the effective velocity component concerning the 2D section. The scaling of the Mach and Reynolds numbers, resulting from Eq. (2), is given by:

$$M_{\infty,2D} = M_{\infty,3D} \cos \Lambda_s \quad Re_{\infty,2D} = Re_{\infty,3D} \cos^2 \Lambda_s \quad (3)$$

The corresponding values are reported in Table 2 for nominal cruise conditions. Finally, an angle of attack equal to 2.15 deg has been selected for the 2D analysis to yield the best agreement with the pressure coefficient distribution from the full 3D wing results obtained in nominal cruise conditions. The corresponding comparison between 2D and three-dimensional (3D) pressure coefficients is

Table 1 Airflow properties in cruise conditions for the DLR-F25 wing

Density, kg/m ³	Temperature, K	Velocity, m/s	Viscosity, kg/(m · s)
0.3955	220.80	232.26	$1.4443 \cdot 10^{-5}$

Table 2 Mach and Reynolds numbers for the DLR-F25 full 3D wing and effective values for two-dimensional analysis at $y/b = 0.85$

Geometry	Mach number, M_∞	Reynolds number, Re_∞
3D wing	0.780	$8.27 \cdot 10^6$
2D section (85% span)	0.714	$6.93 \cdot 10^6$

reported in Fig. 3, where the 3D sectional distribution is scaled by $1/\cos^2(\Lambda_s)$, as required by the swept wing theory [33]. The dashed black line in Fig. 3 represents the critical pressure coefficient associated with incipient sonic flow, which is evaluated here by using Anderson's formulation [34],

$$C_{p,crit} = \frac{2}{\gamma M_\infty^2} \left\{ \left[\frac{2 + (\gamma - 1)M_\infty^2}{\gamma + 1} \right]^{\gamma/(\gamma-1)} - 1 \right\} \quad (4)$$

where $\gamma = 1.4$ and $M_\infty = M_{\infty,2D}$. In the remainder of the paper, all the relevant airflow and wing geometry properties will be directly referred to the transformed values for the 2D analysis, omitting the 2D subscript.

It is worth mentioning that the described approach, often referred to as the 2.5D method, can only provide approximate results for a tapered swept wing, where the local sweep angle varies from the leading edge to the trailing edge [35]. In Eqs. (1–3), the sweep angle Λ_s is referred to 40% of the chord length, the expected shock location in nominal cruise conditions, because previous studies have shown

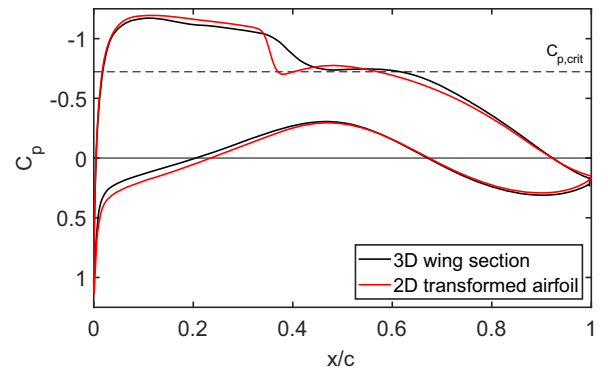


Fig. 3 Pressure coefficient distribution for the DLR-F25 wing section at $y/b = 0.85$: 3D wing section (scaled by $1/\cos(\Lambda_s)$) vs 2D transformed airfoil.

that this leads to a better agreement with the targeted 3D pressure distribution on the wing section [36]. While more advanced techniques, including the 2.75D method [33,35,36], can be applied to the investigation of these wings, this approximated approach has been deemed acceptable for the present study, whose main scope is the investigation of the SVG effects on a typical supercritical airfoil. Therefore, the results described in this paper are not meant to be representative of the actual behavior of the DLR-F25 wing.

B. Geometry, Mesh, and Simulation Settings

The geometry of the selected DLR-F25 wing section, as well as the computational domain required for the CFD analysis, were modeled in Ansys Design Modeler®. The length and height of the fluid computational domain were set to 100 times the chord length of the wing section, according to the geometry shown in Fig. 4, to minimize the effect of the far-field boundary conditions on the simulations. The meshing process was performed within Ansys Workbench®. To improve the accuracy of the solutions, a structured, C-grid mesh was realized, as presented in Fig. 4, and the mesh quality was ensured by following the best-practice recommendations for Ansys CFD provided in [37]. To appropriately resolve the boundary layer, the height of the cells adjacent to the airfoil surface was set to $5 \cdot 10^{-6}$ m, resulting in $y^+ < 1$. The SVG was modeled as a zero-thickness wall normal to the airfoil upper surface, with parametric height and chordwise position. The discretization of the fluid domain was carried out enforcing the presence of 40 elements along this wall, regardless of the SVG height. The final mesh contained about $2.5 \cdot 10^5$ volumes.

CFD simulations were performed in the Ansys Fluent® software. The fluid domain was modeled as a compressible ideal gas, whose properties are listed in Table 1. Turbulence was modeled selecting the $k-\omega$ Shear Stress Transport (SST) model [38,39], while no-slip

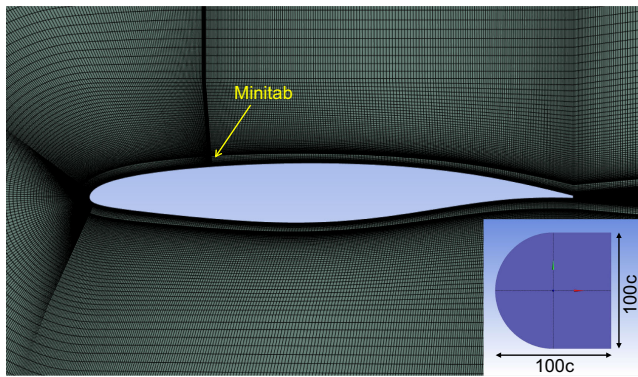
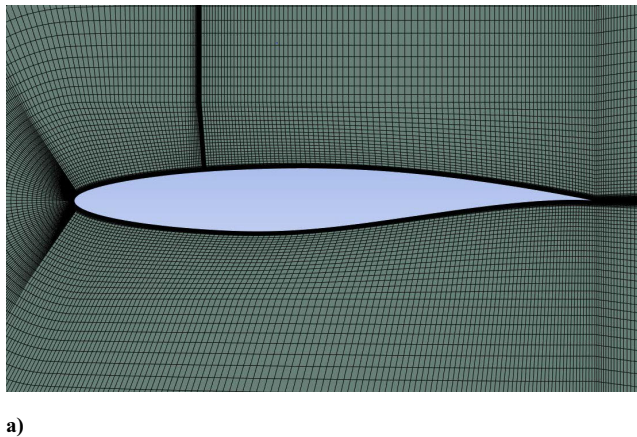


Fig. 4 Structured mesh around the DLR-F25 wing section at $y/b = 0.85$, with minitab of height $h/c = 0.20$ at $x^*/c = 0.25$ and computational domain.



a)

wall boundary conditions were imposed on the airfoil and minitab surfaces. The CFD solver was configured to use a pressure-based formulation with second-order spatial discretization. Simulations were run in two different steps. First, a stationary analysis was conducted, setting the residual convergence requirements to $1 \cdot 10^{-5}$ for the lift, drag, moment coefficients, and wall shear stress as a convergence criterion. Second, if the convergence was not achieved within 1000 iterations, implicit transient simulations were run using the obtained stationary solution as an initial guess, with a time step of 1 ms.

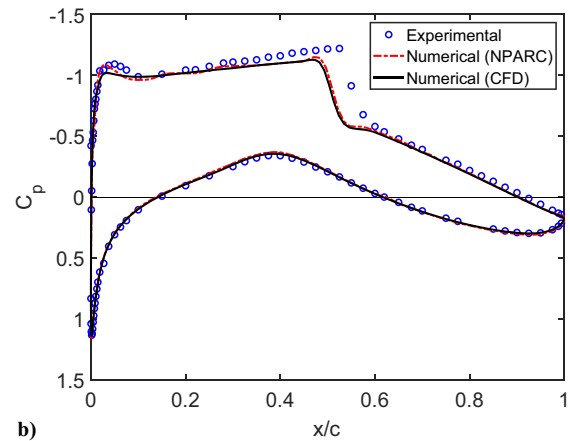
C. Experimental Validation

The validity of the methodology proposed in this paper for investigating the effects induced by the spoiler configuration of the SVG on a supercritical airfoil was tested by comparing the results from CFD simulations with existing experimental data. Because, to the best of the authors' knowledge, no experimental data are available in the literature for supercritical airfoils equipped with a minitab or spoiler on the upper surface and operated at transonic speeds, the following cases were selected: 1) the clean configuration of a RAE 2822 supercritical airfoil, at transonic speeds and small incidence angle, and 2) a NACA 0012 airfoil with a minitab of varying sizes, mounted on the upper surface at different chordwise locations, in low-speed flow conditions.

In the first case, the experimental dataset provided by Cook et al. [40] for $M_\infty = 0.729$, $Re_\infty = 6.5 \cdot 10^6$, and an angle of attack equal to 2.31° was considered. The CFD analysis was set up by generating the RAE 2822 airfoil geometry from the coordinates provided in Ref. [40] and discretizing the computational fluid domain according to the procedure described in Sec. II.B. This resulted in a mesh of about $2.1 \cdot 10^5$ volumes, as depicted in Fig. 5a. The simulation was carried out using the airflow conditions specified in Table 3. The resulting pressure distribution is compared to the experimental results in Fig. 5b, in which overall good agreement can be observed. The main discrepancy between the CFD simulation and experimental results lies in the position of the normal shock on the upper surface, which is slightly farther downstream in the experimental tests. However, the shock position from the CFD analysis is in excellent agreement with that determined by Slater using the NPARC code [41]. Further CFD analyses were conducted on the RAE 2822 airfoil under the same conditions reported in Ref. [42] for varying mesh size and using different turbulence models, yielding very similar results to those computed in this paper. Therefore, it can be concluded that the

Table 3 Airflow properties for the RAE 2822 airfoil analysis

Density, kg/m ³	Temperature, K	Velocity, m/s	Viscosity, kg/(m · s)
0.3813	255.56	233.54	$1.6277 \cdot 10^{-5}$



b)

Fig. 5 For the airfoil RAE 2822: a) structured mesh and b) pressure coefficient distributions, evaluated for the flow conditions in Table 3.

proposed CFD setup is suitable for simulating the aerodynamic behavior of a typical supercritical airfoil in transonic flow conditions.

The second step of the experimental validation aims at verifying the suitability of the proposed methodology for analyzing the aerodynamic effects introduced by the presence of a minitab on the upper surface of the airfoil, for varying vortex vane heights and chordwise positions. This task was accomplished by reproducing, through CFD simulations, the experimental results presented by Heathcote et al. [4,15] for a NACA 0012 airfoil. These simulations were performed by generating geometry and mesh according to the procedure described in Sec. II.B (see Fig. 6) and setting the airflow

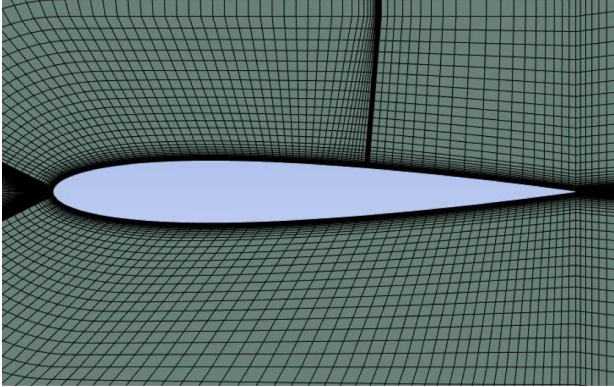


Fig. 6 Structured mesh around the airfoil NACA 0012, with a minitab of height $h/c = 0.40$ positioned on the upper surface at 60% of the chord line.

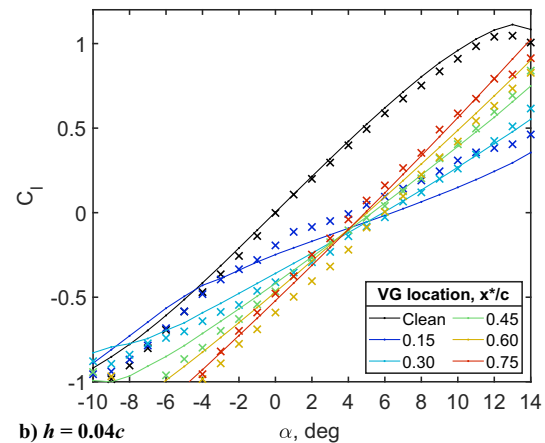
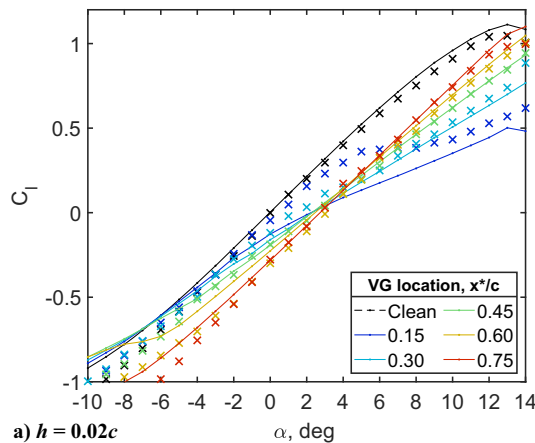


Fig. 7 Lift coefficient vs angle of attack for NACA 0012 airfoil with a minitab of varying height and chordwise position: CFD (lines) vs experimental (markers) results.

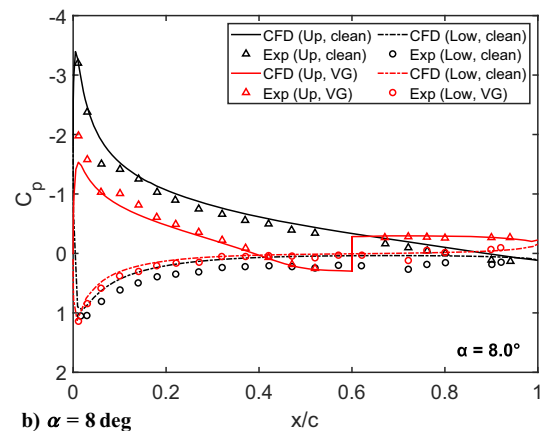
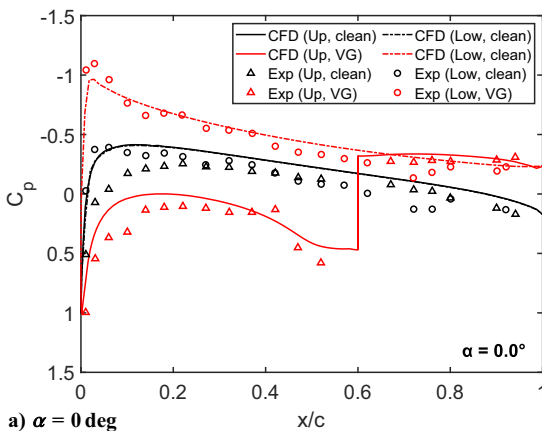


Fig. 8 Pressure coefficient distributions for NACA 0012 airfoil with minitab of height $h = 0.04c$ at $x^* = 0.60c$ and clean configuration: CFD vs experimental (Exp) results.

conditions to the same values indicated by the authors, that is, $U_\infty = 20$ m/s, $Re_\infty = 6.61 \cdot 10^5$, and standard air density and temperature. The minitab heights and locations analyzed were $h/c = [0.02, 0.04]$ and x^*/c ranging from 0.15 to 0.75, respectively. Finally, the angle of attack was varied between -10 and 14 deg.

Figure 7 shows good overall agreement between the experimental and CFD $C_l - \alpha$ curves across all minitab configurations analyzed, as well as for the clean airfoil configuration. The main differences between the numerical and experimental data are observed at large negative angles of attack and for $x^*/c = 0.15$. In the latter case, this discrepancy can be explained by considering that, in the experimental tests, the boundary layer over the airfoil was forced to transition to turbulence at $x/c = 0.1$, by placing a wire on both the upper and lower surfaces. Therefore, it can be supposed that the proximity of the wire to the minitab contributed to the different patterns observed for $x^*/c = 0.15$. To gain further insight into the capability of the CFD setup to reproduce the experimental results, a comparison of the pressure distributions around the airfoil is reported in Fig. 8, showing good agreement for the cases $\alpha = 0$ deg and $\alpha = 8$ deg, both for the clean configuration and for the minitab configuration with height $h = 0.04c$ and position $x^* = 0.25c$. It is worth mentioning that the differences observed between the experimental and numerical results in the clean configuration were already observed by Heathcote et al. [15] and are therefore independent of the proposed CFD approach. Finally, contour plots of the velocity field around the airfoil for the same minitab configuration are displayed in Fig. 9, in the cases $\alpha = 0$ deg and $\alpha = 10$ deg. Here, the boundary of the recirculation region and wake caused by the minitab in the experiments is overlaid on the simulated velocity field, showing excellent agreement. Overall, the presented results demonstrate that the proposed approach can

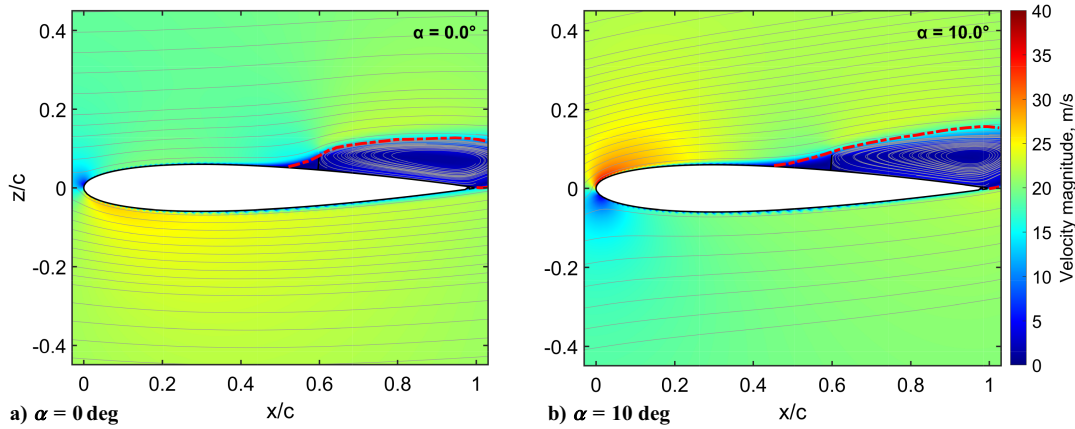


Fig. 9 Computational velocity field around NACA 0012 airfoil, with minitab of height $h = 0.04c$ at $x^* = 0.60c$, experimental boundary of recirculation area (in red).

be used to simulate the aerodynamic behavior induced by the presence of a minitab on the airfoil's upper surface.

III. Sensitivity Analysis of Vortex Generator Height and Chordwise Location in Cruise Conditions

In this section, the aerodynamic effect of introducing a SVG on the upper surface of the DLR-F25 wing section located at $y/b = 0.85$ is assessed in nominal cruise conditions (see Table 1). The analysis is conducted for varying chordwise locations and vane heights of the SVG, according to the methodology described in Sec. II.

A. Effect on Lift and Drag Coefficients

An overview of the SVG effect on lift and drag coefficients is depicted in Fig. 10, for vane heights ranging from $0.005c$ to $0.06c$, and chordwise positions included between $0.1c$ and $0.9c$. The lift and drag coefficients evaluated for the wing section in clean configuration, that is, $C_l = 0.698$ and $C_d = 0.013$, are also reported for reference.

The results presented in these plots clearly show that the introduction of a SVG on the upper surface can significantly impact the aerodynamic forces acting on the wing section, even when its height is only a small fraction of the chord length. In general, increasing the vane height has a clear effect of intensifying the change produced in the aerodynamic forces. At any height equal to or larger than $0.02c$, the C_l values will become negative for most chordwise locations, potentially assuming large absolute values and therefore leading to an excessive negative wing section loading. However, although this would suggest that the use of small SVGs is a better approach to C_l reduction, it is also worth it to stress that these results are limited to a

2D case. Hence, it is expected that the application SVGs on a 3D wing would result in a less pronounced effect.

The choice of the SVG chordwise location can also significantly affect the performance of the wing section. From Fig. 10a, it can be seen that, for most vane heights, the maximum C_l reduction is achieved for locations around 60% of the chord, in good agreement with the findings from Heathcote et al. [4,15], evaluated in subsonic conditions. The lift generated by the wing section will gradually increase as the SVG is moved toward either the leading or the trailing edge. However, Fig. 10a also suggests that this regular behavior is only observed for SVGs whose vane height exceeds a critical value, included between $0.005c$ and $0.01c$ in the present investigation. For smaller heights, the $C_l - x^*/c$ curves present two different patterns: for SVGs located more closely to the leading edge, the lift reduction is very limited and slowly increases for increasing values of x^*/c , while SVGs located farther downstream exhibit the same behavior observed for $h/c \geq 0.01$. The transition between these patterns occurs for smaller values of x^*/c and more sharply as the SVG height is increased, as shown for $h/c = 0.002$ and $h/c = 0.005$. In these cases, the maximum lift reduction is also shifted to farther downstream SVG locations. This peculiar aerodynamic behavior will be discussed and explained later in this section. The maximum drag generation is generally not obtained at the same SVG locations as the maximum lift reduction. In fact, in the $C_d - x^*/c$ curves in Fig. 10b, the maximum C_d is observed for positions between 20 and 30% of the chord length. Therefore, it can be deduced that SVG locations in the second half of the chord length can offer a larger C_l reduction with a limited generation of drag. For SVG locations in proximity of the leading edge, it can be observed that variation of C_l with respect to h/c increases with a decreasing rate as larger heights are approached.

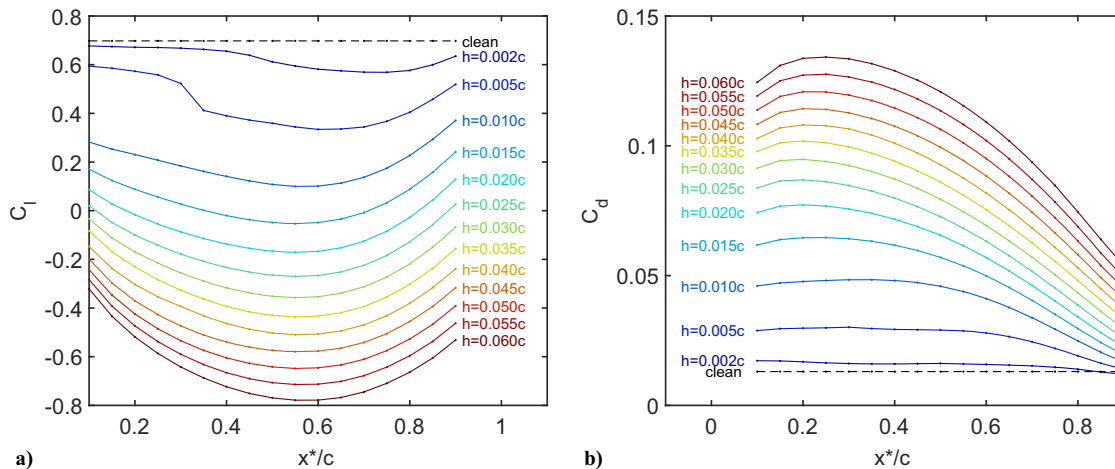


Fig. 10 Effect of minitabs with different vane heights, positioned at varying chordwise locations, on a) lift and b) drag coefficients in nominal cruise conditions.

This behavior is less visible in the $C_d - x^*/c$ curves, leading to the conclusion that higher SVGs can lead to a considerably higher generated drag without offering significant advantages in terms of lift reduction.

B. Effect on Velocity, Pressure, and Skin Friction Coefficients Distribution for Varying SVG Chordwise Location

The patterns described by the C_l and C_d curves for varying height and chordwise locations of the SVG, discussed in the previous subsection for the spoiler configuration, provide a good overview of its impact on the aerodynamic performance of a wing section. To gain further insight on the causes of such aerodynamic effects, a discussion on the alterations introduced by the SVG in the velocity field and pressure distribution is presented in what follows.

Figures 11a and 11b illustrate the pressure and skin friction coefficient distribution along the chord of the investigated wing section in cruise conditions, for varying chordwise locations of a SVG of height $h = 0.01c$. This specific height value has been selected to represent

typical SVG behavior when the vane height exceeds the critical value indicated in Sec. III.A. The velocity fields around the airfoil are shown in Fig. 12 for $x/c = [0.15, 0.30, 0.60, 0.90]$. For reference, the velocity field around the clean wing section is reported in Fig. 13, and the corresponding C_p and C_{fx} distributions are reported in Fig. 11 by means of a continuous black line. The clean wing section exhibits the typical behavior of a supercritical airfoil, with the minimum negative C_p reached in proximity of the leading edge and followed by a pressure plateau until about 40% of the chord, where the shock occurs, as also indicated by the sudden pressure change at approximately $0.4c$. The introduction of a minispoiler changes significantly the pressure distribution and the velocity flow above the upper surface of the airfoil, as described in what follows:

1) Starting from the leading edge, the SVG introduces a deceleration of the airflow, such that supersonic conditions are no longer reached upstream of the SVG, except that for chordwise positions in proximity of the trailing edge (see the case $x^*/c = 0.90$ in Fig. 11a).

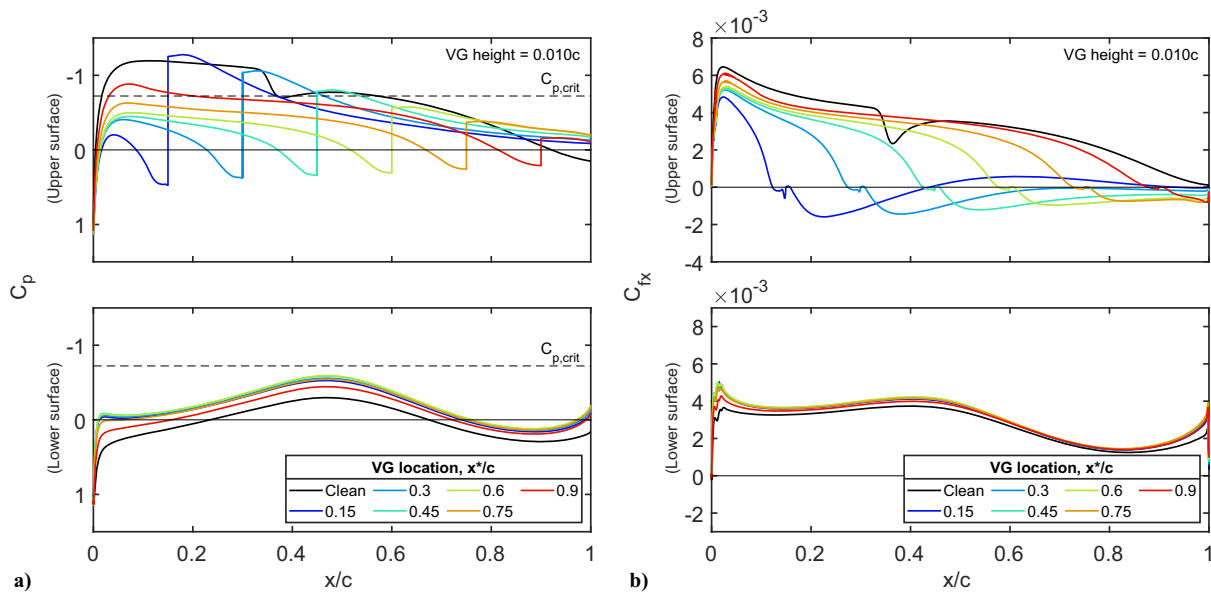


Fig. 11 Effect of minitabs of height $h/c = 0.01$, positioned at varying chordwise locations, on a) pressure and b) skin friction coefficients in nominal cruise conditions.

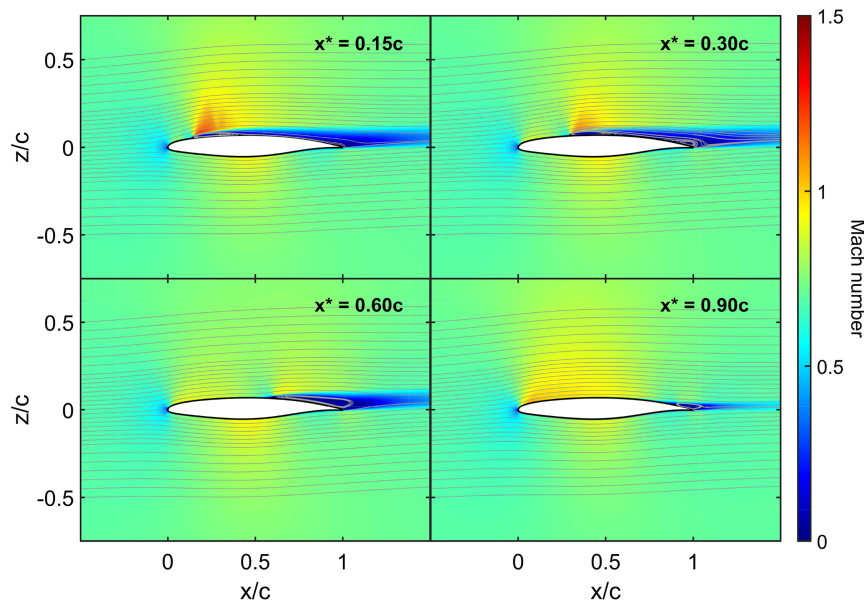


Fig. 12 Effect of minitabs of height $h/c = 0.01$, positioned at varying chordwise locations, on the velocity field around the wing section in nominal cruise conditions.

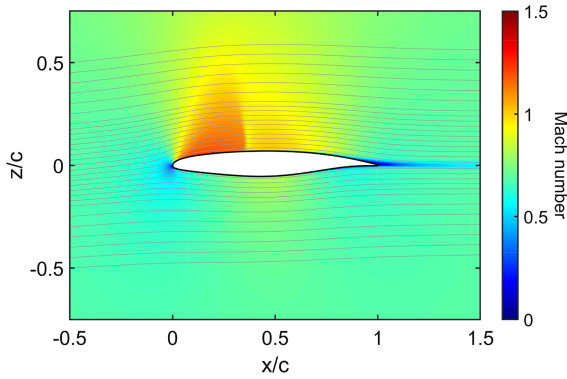


Fig. 13 Velocity field in nominal cruise conditions for the clean configuration of the wing section.

2) This deceleration is followed by a pressure drop across the vortex vane, which gradually decreases as the SVG is moved downstream. Among the cases investigated, only for $x^*/c \leq 0.45$ this pressure drop is such to lead to supersonic conditions downstream of the SVG, as indicated by the crossing of the $C_{p,crit}$ line. The expansion of the airflow around the minispoiler is also very visible in Fig. 12 (see, e.g., the case $x^*/c = 0.15$).

3) One of the main effects of the SVG on the airflow pattern is the introduction of recirculation zones, whose location and extension are indicated by the $C_{fx} < 0$ values in Fig. 11b. Here, it can be observed that the SVG triggers a small recirculation zone upstream and, more importantly, a larger one downstream. For $h/c = 0.01$, the latter recirculation area extends from the minitab to the trailing edge in most cases, with flow reattachment only observed for $x^*/c = 0.15$. This behavior is also visible in Fig. 12, in which the streamlines clearly show how the recirculation area gradually extends toward the trailing edge (up to $x^*/c = 0.30$) and hence becomes smaller and smaller as the SVG is moved farther downstream, reducing the height of the wake region. This process explains why the maximum generated drag is achieved around $x^*/c = 0.30$ for a SVG of height $0.01c$ (see Fig. 10b).

More limited effects by the SVG can be observed on the lower surface of the wing section. In fact, as can be seen in Fig. 11a, the overall evolution of the C_p and C_{fx} distributions along the chord is not strongly affected by the parameter x^*/c . However, it is also possible to observe that the presence of the SVG leads to lower pressures on the lower surfaces, with the maximum pressure reduction observed for the

$x^*/c = 0.60$ case among those investigated, in agreement with the maximum C_l reduction already observed in Fig. 10a.

C. Effect on Velocity, Pressure, and Skin Friction Coefficients Distribution for Varying SVG Height

The pressure and skin friction coefficient distributions along the chord of the airfoil are depicted in Figs. 14a and 14b for varying heights of the SVG vane and $x^*/c = 0.25$. The clean configuration of airfoil is also included in the plots for reference. The corresponding velocity flowfields are illustrated in Fig. 15 for $h/c = [0.005, 0.01, 0.02, 0.04]$. Overall, these plots clearly show the strong impact of the VG height on the aerodynamic behavior of the wing section, as detailed in the following annotations:

1) On the upper surface, for vane heights below the critical height (see, e.g., $h/c = 0.002$), the location of the shock wave is moved upstream with respect to the clean configuration, with a reduction of its intensity. For $h/c \geq 0.01$, supersonic conditions are no longer reached in this region, as already discussed in the previous subsection.

2) The airflow patterns after the pressure drop across the SVG are severely affected by its vane height. Although increasing h/c above 0.01 has the expected effect of enlarging the height of the downstream recirculation and wake regions, smaller SVGs can also significantly affect the velocity flowfield above the upper surface. In fact, for $h/c = 0.002$ and 0.005, the pressure drop becomes particularly significant (see Fig. 14a), leading to very high velocities ($M > 1.5$), as visible in Fig. 15. In this case, as also indicated by the C_{fx} patterns in Fig. 14b, the flow reattaches to the upper surface almost immediately downstream of the SVG. This phenomenon explains the different pattern shown by the $C_l - x^*/c$ curves in Fig. 10 for small SVG heights and locations in the first portion of the airfoil chord. Figure 16 shows how, for $h/c = 0.005$, the intensity of the supersonic region generated by minitabs located at $x^*/c \geq 0.40$ is no longer such to enforce the flow reattachment. Therefore, the aerodynamic behavior becomes similar to that presented by SVGs of height $h \geq 0.01c$.

3) On the lower surface, the acceleration induced by higher SVGs leads to supersonic speeds starting from the case $h/c = 0.02$, as shown by the C_p distribution in Fig. 14a. For larger vane heights, the formation of the supersonic regions is also very visible in Fig. 15 (see $h/c = 0.04$). In particular, a small supersonic region is located in proximity of the leading edge, and a second, more extensive region can be observed around the middle of the chord. Both regions terminate with normal shock waves, whose locations is shifted farther

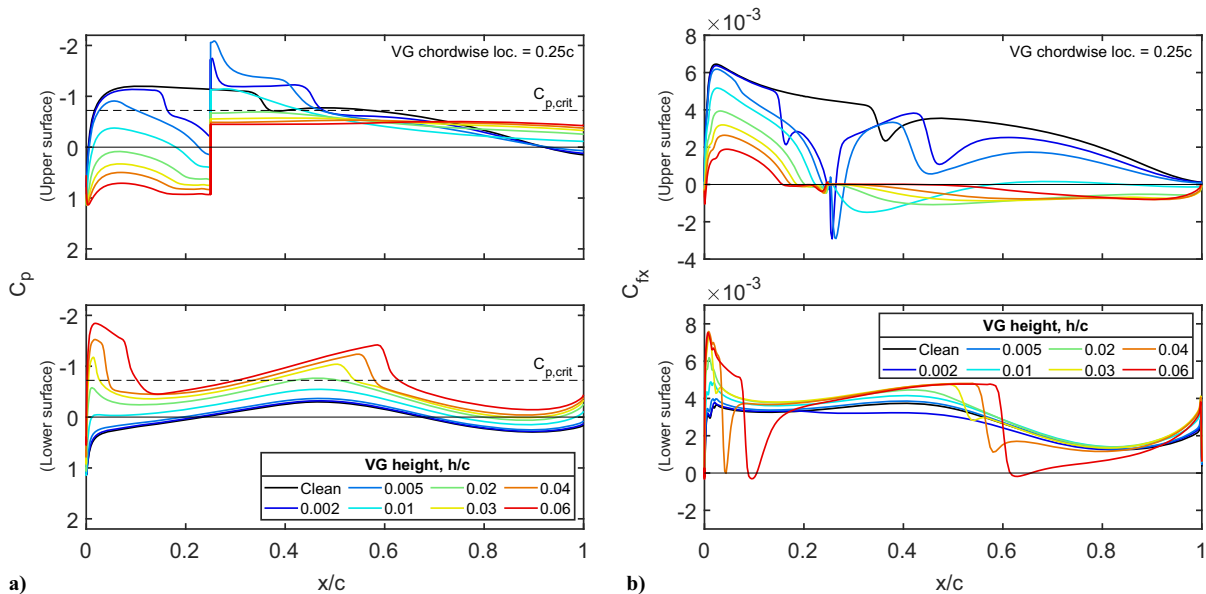


Fig. 14 Effect of minitabs of varying height, positioned at $x^*/c = 0.25$, on a) pressure and b) skin friction coefficients in nominal cruise conditions.

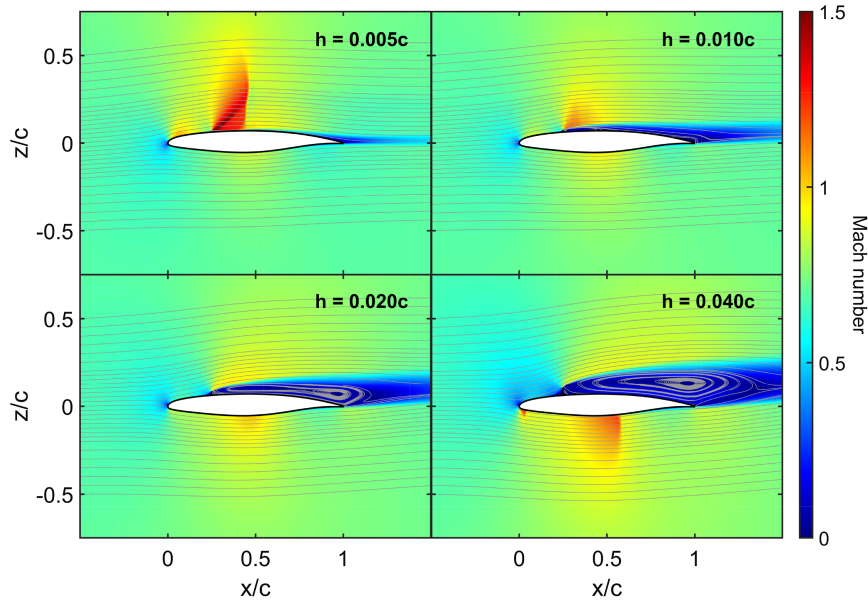


Fig. 15 Effect of minitabs of varying height, positioned at $x^*/c = 0.25$, on the velocity field around the wing section in nominal cruise conditions.

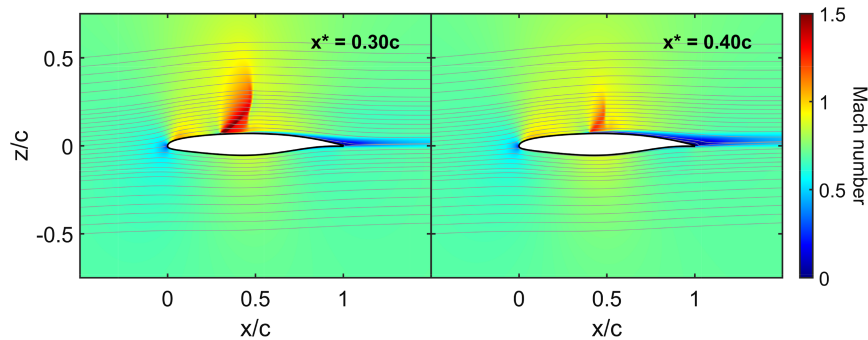


Fig. 16 Velocity field around the wing section in nominal cruise conditions, with a minitab of height $h/c = 0.005$ and varying chordwise position.

downstream as h/c is increased. In Fig. 14b, the case $h/c = 0.06$ suggests that shock-induced separation occurs for higher SVGs.

In conclusion, the presence of a SVG on the upper surface of a wing section in transonic conditions can effectively alter its aerodynamic performance, leading to drastic changes in lift and drag coefficients. The intensity of these variations will generally be stronger for larger SVG heights, while the maximum lift reduction is achieved for positions around 60% of the chord length. Although the SVG impact on the aerodynamic coefficients can be used to achieve load control and alleviation, it was also shown that higher SVGs ($h/c \geq 0.03$) can lead to undesirable effects such as large negative C_l values and the formation of normal shock waves on the airfoil lower surface. On the other hand, small SVGs ($h/c < 0.01$) can also generate strong shock waves on the upper surface. Therefore, the selection of the vane height appears to be a crucial factor in the SVG design process. Nonetheless, it is also worth considering that the presented results are limited to the investigation of a 2D section and that the effect of the application of either one or multiple SVGs on a full 3D wing are supposed to be significantly milder, hence reducing these potential negative effects.

IV. Sensitivity Analysis of Angle of Attack Effects on Vortex Generator Performance

In the previous section, the effects of the SVG in spoiler configuration on the aerodynamic behavior of an outer wing section have been investigated in nominal cruise conditions, hence keeping the angle of attack constant at 2.15 deg. While this corresponds to the main operative condition for the spoiler function of the SVG, it is also important to establish how its performance changes for varying

incidence, because different angles of attack could be induced by gusts or maneuvers. As in the previous analyses, the effect of varying α will be assessed for varying height and chordwise location of the SVG, in the ranges specified in Sec. III.

A. Aerodynamic Effects for Varying SVG Chordwise Location

The lift and drag coefficient curves, evaluated for angles of attack ranging from -5 to 10 deg, are depicted in Figs. 17a and 17b for different chordwise locations of a SVG of height $h/c = 0.02$. In the clean configuration, reported in these plots for reference as a dashed black line, the wing section exhibits a linear increase of C_l between $\alpha = -5$ deg and $\alpha = 3$ deg, with stall occurring at about $\alpha = 5$ deg. The drag coefficient of the section, in the absence of the SVG, has its minimum in the range between -2 and 2 deg, with larger values for smaller and larger angles of attack, as expected. The introduction of a minitab of height $0.02c$ on the upper surface can significantly change the patterns exhibited by lift and drag for varying angle of attack, as explained in what follows:

1) An important effect of the SVG is the change of slope in the linear range of the $C_l - \alpha$ curves, which increases with the parameter x^*/c . SVGs located in the first portion of chord, up to 60% of the chord length, reduce the lift variation with the angle of attack with respect to the clean configuration case, while SVGs positioned more closely to the trailing edge lead to a sharper increase of C_l for increasing α . It is also worth mentioning that, while this central portion of the $C_l - \alpha$ curves will be referred to as linear range in the following discussion, the C_l evolution also becomes more nonlinear for SVG locations near the leading edge.

2) In the linear range, the generated drag presents a significant increase with the angle of attack for SVG locations closer to the

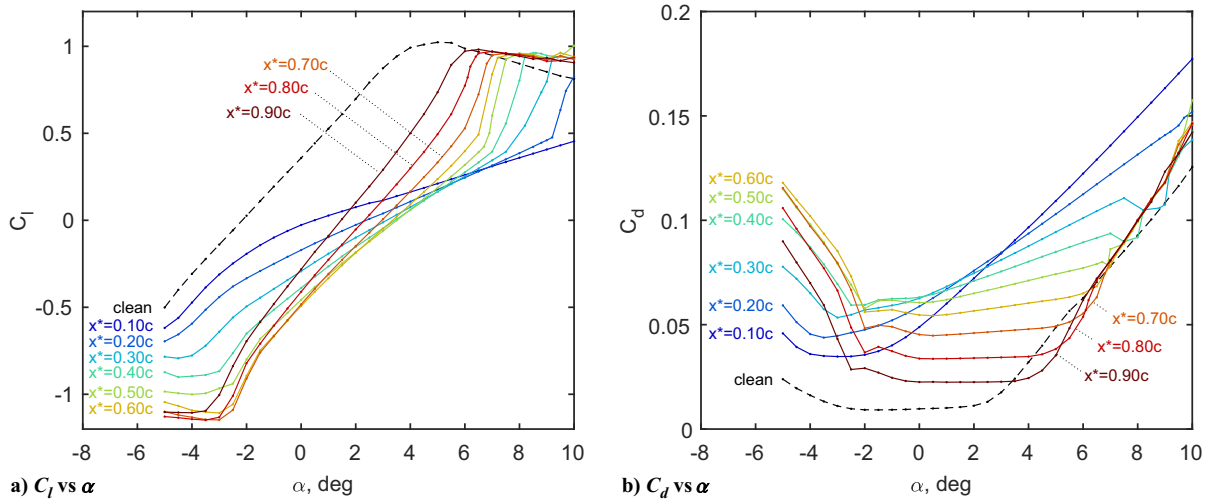


Fig. 17 Effect of minitabs of height $h = 0.02c$, with different chordwise positions, on a) lift and b) drag coefficients for varying angle of attack.

leading edge, while remaining almost constant for locations in proximity of the trailing edge (see Fig. 17b).

3) At high incidence, the SVG delays the stall of the airfoil. This effect becomes more significant as the SVG is moved toward the leading edge, with stall occurring at about $\alpha = 6.5$ deg for $x^*/c = 0.90$ and out of the investigated range for $x^*/c = 0.10$. However, it is also worth mentioning that the transition from the linear behavior to stall occurs more and more sharply as the SVG approaches the leading edge (see Fig. 17a).

4) At negative angles of attack, the SVG can lead to an earlier stall onset than in clean configuration. While this effect appears to be very mild for SVGs positioned near the leading edge, it gradually becomes more significant, with negative stall occurring at $\alpha = -2$ deg in the worst case, that is, for locations around 60–70% of the chord length. Sharper transitions between the linear range and stall at negative incidence are observed for SVGs locations in proximity of the trailing edge.

To offer a further insight into the aerodynamic behavior induced by SVGs located at different chordwise positions, the pressure and skin friction coefficients distributions, as well as the velocity field, are reported here for two different angles of attack, $\alpha = 5$ deg and $\alpha = -1$ deg. These specific values have been selected to elucidate the effects of varying incidence within the linear range, while the SVG impact on the stall onset and other transitions will be analyzed in Sec. IV.B.

The pressure and skin friction distributions, plotted in Fig. 18 for $\alpha = 5$ deg, clearly show the limited impact of SVGs located in proximity of the trailing edge, which results in the smaller lift reduction and generated drag highlighted in Fig. 17. In this case, as also visible in Fig. 19 for $x^*/c = 0.80$, the primary effect from the SVG is the shifting of the shock location farther upstream on the upper surface, with a reduction of its intensity. As the SVG is moved toward the leading edge, it can be observed that the separated region and the wake become larger and larger, accounting for the increase in generated drag, while supersonic conditions are no longer reached on the upper surface. At the same time, larger airflow acceleration is observed along the lower surface, explaining the larger lift reduction observed for SVG locations near the leading edge at high angles of attack.

In the case $\alpha = -1$ deg, the pressure and skin friction coefficients presented in Fig. 20 highlight how the most significant SVG effects are produced on the airfoil lower surface. In fact, differently from the clean configuration case, supersonic regions appear in the presence of the SVGs at any chordwise locations. In particular, a first small supersonic region is located in proximity of the leading edge, while a second larger region can be observed around the middle of the chord line (see the velocity contour plots in Fig. 21). Normal shock waves are present at the end of the former supersonic region upstream in all the cases investigated but only visible for $x^*/c \geq 0.3$ for the latter

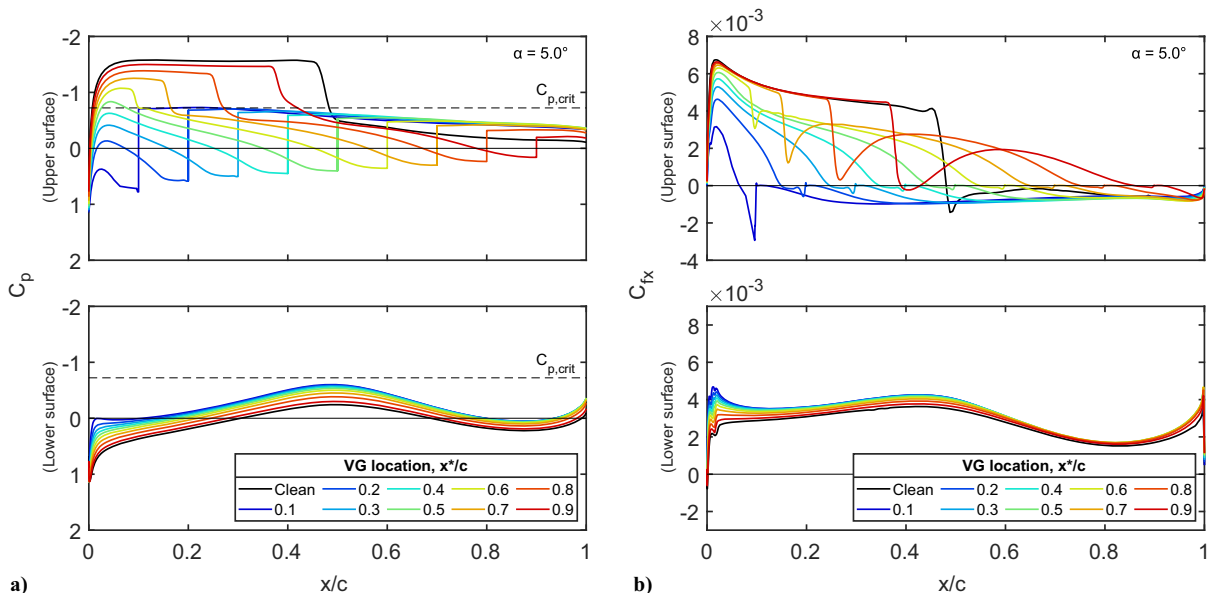


Fig. 18 Effect of minitabs of height $h = 0.02c$, with different chordwise positions, on a) pressure and b) skin friction coefficients for $\alpha = 5$ deg.

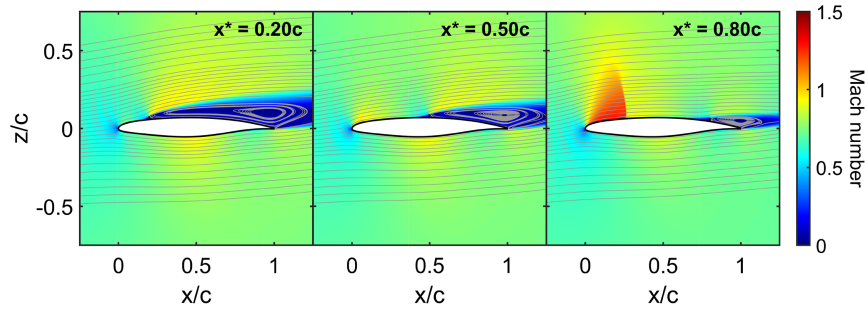


Fig. 19 Effect of minitabs of height $h = 0.02c$, with different chordwise positions, on the velocity field around the wing section for $\alpha = 5^\circ$.

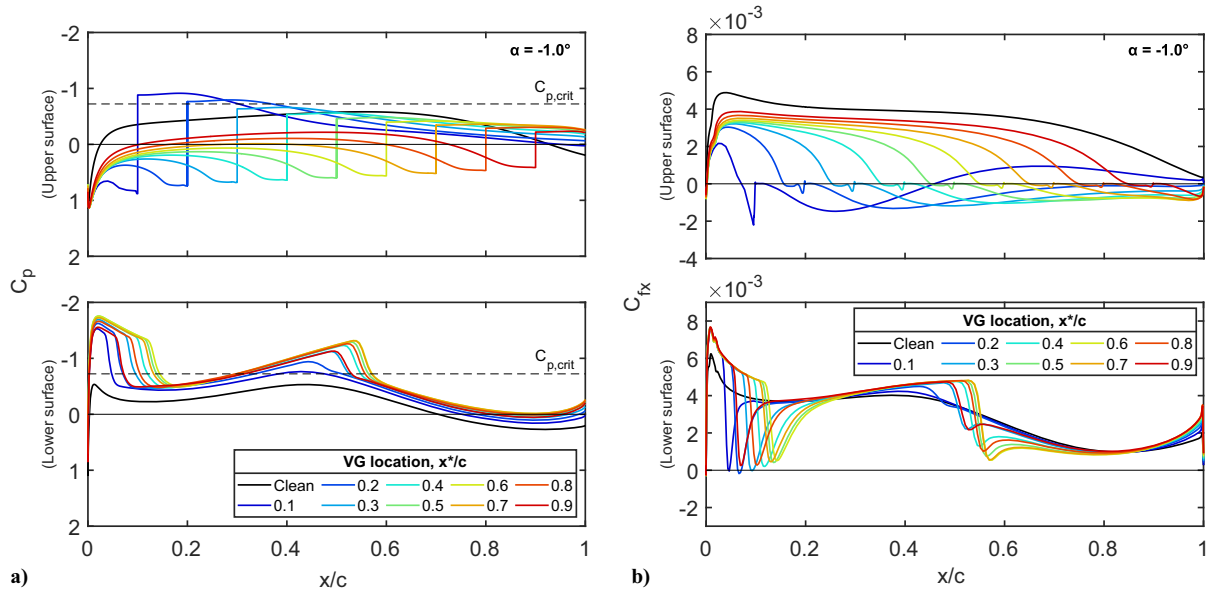


Fig. 20 Effect of minitabs of height $h = 0.02c$, with different chordwise positions, on a) pressure and b) skin friction coefficients for $\alpha = -1^\circ$.

region downstream. For both shock waves, the strongest intensity and the farthest downstream locations are observed for SVG positions around the 60% of the chord length, in agreement with the maximum C_l reduction achieved in this case (see Fig. 17).

B. Aerodynamic Effects for Varying SVG Height

The lift and drag coefficient curves obtained for varying angle of attack and different vane height are illustrated in Fig. 22 in the case of a SVG located at 25% of the chord length. In additions to the behaviors described in Sec. IV.A, these curves also exhibit further transitions and peculiar patterns, which are detailed in the following observations:

1) In the linear range, the $C_l - \alpha$ curves corresponding to vane heights larger than $0.01c$ present the same slope, independently of the height value. Consistently with the previous discussion, this slope is smaller than that observed in the absence of the SVG. The

curves corresponding to $h/c = 0.005$ and 0.01 present a gradual variation between the slopes observed in the clean configuration and for $h/c > 0.01$. Figure 22a also shows that the increase of the lift coefficient with α has a pronounced nonlinear trend for these two vane height values.

2) At higher angles of attack, the linear range does not always terminate with a sharp increase in C_l followed by stall, as observed in the case $h/c = 0.02$. For instance, at $h/c = 0.01$, the sudden lift increase is followed by a further linear range, terminating with stall at $\alpha \cong 9^\circ$. In the $C_l - \alpha$ curve corresponding to $h/c = 0.005$, i) the linear range is followed, from $\alpha \cong 1.5^\circ$, by a slow nonlinear increase in C_l ; ii) at $\alpha \cong 4^\circ$, there is a further, sharper increase in C_l , followed by a sudden decrease at $\alpha \cong 6^\circ$; and iii) a further linear increase is observed between the latter transition and $\alpha \cong 8^\circ$, when stall occurs. Nonetheless, these additional transitions do not appear to affect the generated drag, as visible in Fig. 22b.

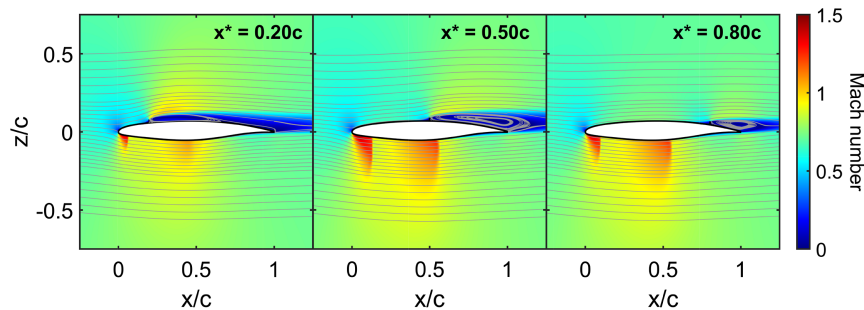


Fig. 21 Effect of minitabs of height $h = 0.02c$, with different chordwise positions, on the velocity field around the wing section for $\alpha = -1^\circ$.

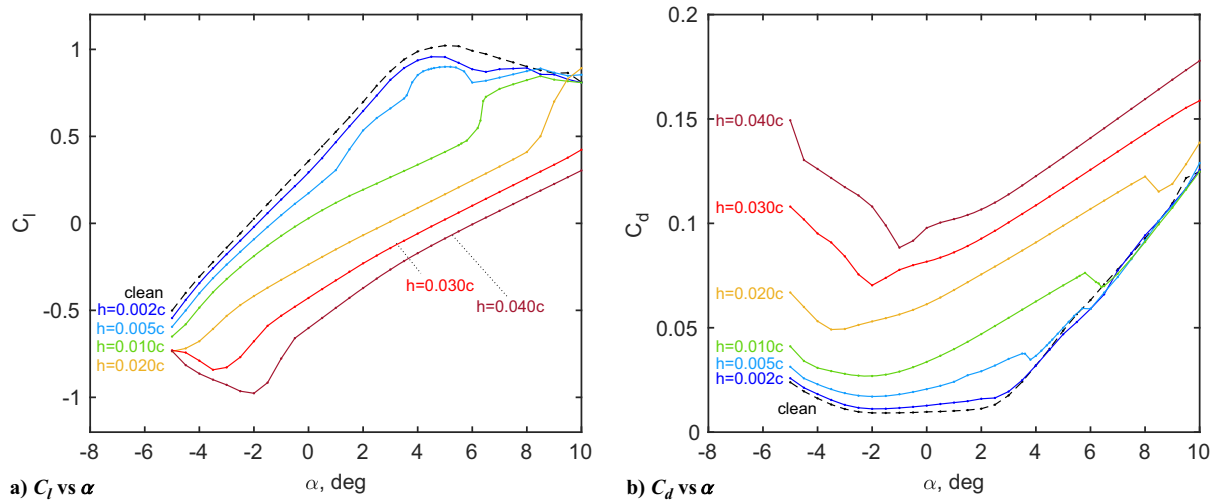


Fig. 22 Effect of minitabs of different vane heights, positioned at $x^*/c = 0.25$, on a) lift and b) drag coefficients for varying angle of attack.

3) At negative incidence, stall can occur significantly earlier (e.g., at $\alpha \cong -2$ deg for $h/c = 0.04$). As the vane height is increased, it is also possible to observe a sharper and sharper fall in the C_l values before the stall onset.

The previously described transitions in the aerodynamic behavior can be explained by observing the contour plots of the velocity fields illustrated in Figs. 23–25. Figure 23 shows the evolution of the velocity field before ($\alpha = 5.5$) and after ($\alpha = 6.5$) the sudden increase of C_l displayed in Fig. 22a for $h/c = 0.01$. It is clearly visible that the reason for this transition lies in the appearance of a normal shock wave in proximity of the leading edge, followed by shock-induced separation. The increase in C_l is not only due to the larger airflow velocities achieved on the first portion of the upper surface but also to a loss of effectiveness of the SVG, which is now mostly immersed in the separated region. At the same time, the height of the wake region appears to decrease across the transition, motivating the reduction in generated drag observed in Fig. 22b. If the angle of attack is further increased, the SVG will become fully immersed in the separated region, and therefore C_l and C_d will eventually approach their clean configuration values.

The presence of additional transitions in the case $h/c = 0.005$ is explained by the velocity fields around the airfoil reported in Fig. 24 for $\alpha = [3.5, 4.5, 6, 9]$ deg. Although the presence of a supersonic region between the SVG and the middle of the chord length in the case $\alpha = 3.5$ deg has already been discussed in Sec. III and illustrated in Figs. 15 and 16, a further supersonic area is also visible in proximity of the leading edge. The first nonlinear increase of C_l observed for $h/c = 0.005$ is due to the gradual onset of the normal shock wave visible at the end of this region, in a process similar to that described for the case $h/c = 0.01$. However, as the angle of attack is further increased, this shock wave will move downstream, eventually leading to a coalescence of the two supersonic regions, which is very visible for $\alpha = 6$ deg. During this phase, where two strong, normal shock waves are still present (see $\alpha = 4.5$ deg in Fig. 24),

the $C_l - \alpha$ curve exhibits a further increase. However, after the complete coalescence of the supersonic regions, which leads to a sudden C_l reduction, the remaining normal shock wave will gradually move toward the leading edge, with the already discussed progressive immersion of the SVG in the separated region following the shock.

Finally, the early onset of negative stall in the presence of high SVGs can be explained by looking at Fig. 25, in which the velocity field contour plots are illustrated for $\alpha = 0$ and $\alpha = -2$ deg in the case $h/c = 0.04$. By comparing the velocity fields at an incidence of 0 deg and 2.15 deg (shown in Fig. 15), it is possible to see that the supersonic region originating in the latter case near the leading edge gradually extends downstream, eventually leading to a normal shock on the lower surface. The formation of this shock wave, besides the shock present in both cases around 60% of the chord length, accounts for the sudden decrease of C_l , observed in Fig. 22a when α is decreased below 0 deg. When $\alpha \cong -2$ deg, these two supersonic regions merge, forming a unique supersonic area extending from the leading edge to about the middle of the chord length, as shown in Fig. 25. The airflow is here strongly accelerated at the leading edge, reaching high speeds above $M = 1.5$ and leading to a strong lift reduction. If the angle of attack is further decreased, the remaining shock wave moves toward the leading edge and gradually loses its intensity. This leads to the higher C_l values displayed in Fig. 22a for $\alpha < 2$ deg. The generated drag rapidly increases after the coalescence of the supersonic regions, due to shock-induced separation and the consequent enlargement of the wake region downstream.

In summary, the analysis conducted in this section has shown that SVGs located at smaller percentages of the chord length offer more robust performances with respect to variations of the angle of attack. Differently, SVGs positioned more closely to the trailing edge cause sharper variations in the lift generated by the wing section for varying incidence, tend to generate potentially strong shock waves, and can lead to stall onset at smaller absolute angles of attack. SVGs whose vane height is between 1 and 2% of the chord length appear to

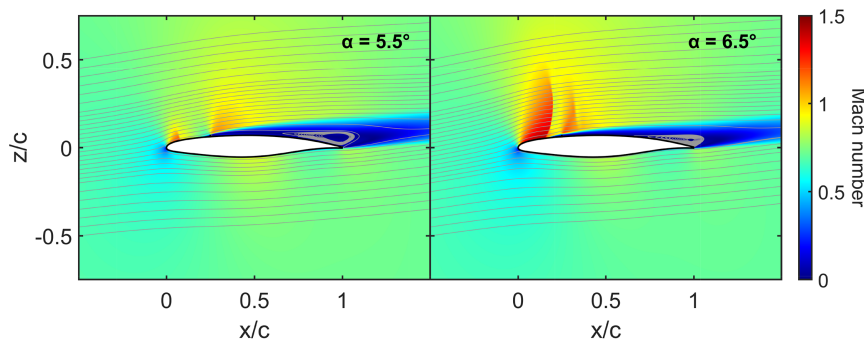


Fig. 23 Effect of a minitab of height $h = 0.01c$, positioned at $x^*/c = 0.25$, on the velocity field around the wing section.

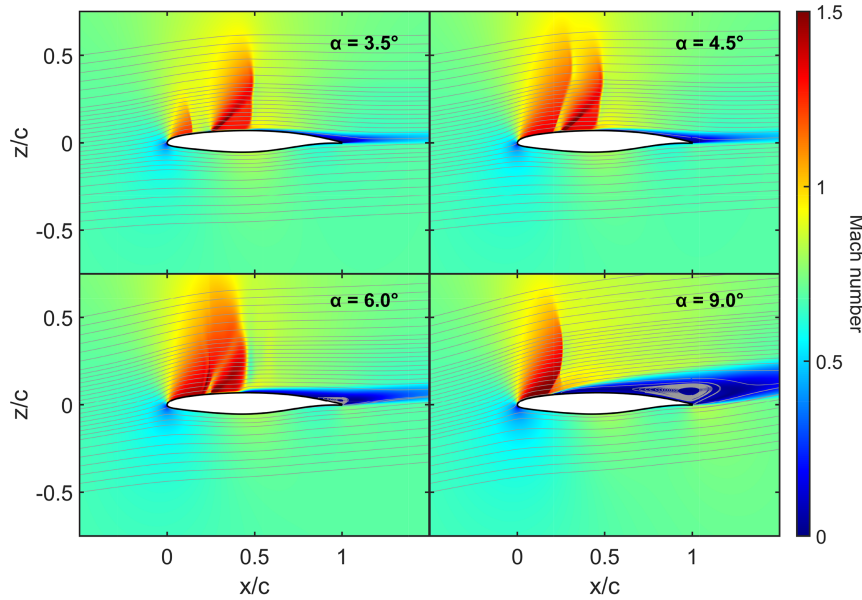


Fig. 24 Effect of a minitab of height $h = 0.005c$, positioned at $x^*/c = 0.25$, on the velocity field around the wing section.

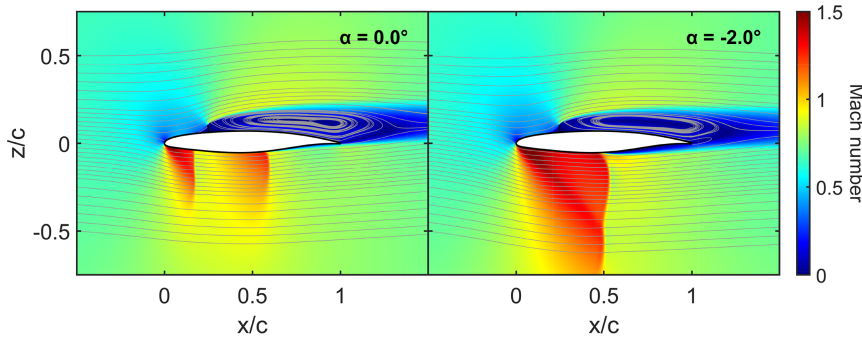


Fig. 25 Effect of a minitab of height $h = 0.04c$, positioned at $x^*/c = 0.25$, on the velocity field around the wing section.

offer good performances in a larger range of angles of attack. In fact, although higher SVGs perform poorly at negative incidence, generating strong shock waves on the lower surface and early stall onset, small SVGs also present complex behavior at higher angles of attack, characterized by the formation of shock waves on the upper surface and sudden variations in the lift reduction.

V. Conclusions

In this paper, the effect of introducing a switchable vortex generator, operating as a minitab, on the upper surface of an airfoil has been investigated in transonic conditions. In particular, the aerodynamic performance of an outer section of the DLR-F25 wing has been explored for varying vane heights and chordwise locations of the vortex generator in nominal cruise conditions and for varying angle of attack.

This study, conducted by means of 2D computational fluid dynamics analyses, has proven that the spoiler configuration of the SVG can effectively reduce the lift generated by the wing section and, more in general, lead to a significant variation of the produced aerodynamic forces. In cruise conditions, lift reduction can be increased by selecting higher SVGs and by positioning them around 60% of the chord length. However, high performances in lift reduction are not always desirable because they can lead to excessive negative wing loading and are often related with the formation of shock waves on the airfoil lower surface. The drag generated by the SVG does not generally follow the same patterns described by the change in lift. While increasing with the SVG height, the maximum C_d values have been observed between 20 and 30% of the chord length. The sensitivity analysis carried out for varying angle of attack has shown that SVGs

located in proximity of the leading edge generally offer more robust performances than those located farther downstream. In fact, SVGs located after 60% of the chord length can lead to sharper lift variations, generation of strong shock waves and early stall onset. Independently of the chordwise position, the introduction of SVGs delays the stall onset at high angles of attack but leads to earlier stalls for negative incidence. Additionally, it has been observed that large SVGs, whose height is equal or above 3% of the chord length, perform poorly at negative incidence, generating strong, normal shock waves on the lower surface and causing stall to occur at smaller absolute values of the angle of attack. On the other hand, small SVGs, whose height is below 1% of the chord length, exhibited limited performance in nominal cruise conditions and at high incidence, particularly if placed within the first portion of the chord length. In these cases, they often induce a significant flow acceleration downstream, leading to the generation of strong, normal shock waves on the upper surface and preventing any significant flow separation.

Overall, the results of the parametric study presented in this contribution indicate that, although the spoiler function of the SVGs has great potential for purposes such as load control and alleviation in transonic conditions, certain combinations of their vane height and chordwise position can also lead to undesirable effects, including the generation of strong shock waves and shock-induced separation. These phenomena can lead to excessive vibrations and have structural implications (e.g., fatigue issues) as well as a significant increase in generated drag. Therefore, a careful selection of these parameters is advised during the design process, which should aim to also determine the optimal balance between load alleviation performance of the SVG and aerodynamic robustness. It is also worth underlining that the presented results are restricted to the case

of a 2D wing section and to the assumption of stationary conditions. Future work will focus on extending these findings to the case of a full 3D wing, hence also investigating the effects of parameters such as the length and the spanwise location of the SVGs. Moreover, further research will be required to fully assess the suitability of SVGs for purposes such as gust load alleviation as well as to analyze the impact of dynamic effects introduced by unsteady airfoil motions, gusts, and continuous turbulence on the SVG load alleviation performance.

Acknowledgments

The work presented herein has been partially funded by the European Community's Clean Aviation program under grant agreement 101101974. The Ultra-Performance Wing project is a project funded under the topic Climate, Energy and Mobility, involving 26 partners. The project started on 1 January 2023. The DLR-F25 configuration has been used for the initial design within the Ultra-Performance Wing project. The authors would like to thank DLR, German Aerospace Center for providing the DLR-F25 test case. The development of the DLR-F25 configuration is funded by the German Federal Ministry for Economic Affairs and Climate Action as part of the LuFo VI-2 project VIRENfrei (funding reference 20X2106B). Views and opinions expressed are those of the authors only and do not necessarily reflect those of the European Union or Clean Aviation Joint Undertaking. Neither the European Union nor the granting authority can be held responsible for them.

References

- [1] Regan, C., and Jutte, C., "Survey of Applications of Active Control Technology for Gust Alleviation and New Challenges for Lighter-Weight Aircraft," NASA TM 2012-216008, 2012.
- [2] Xu, J., and Kroo, I., "Aircraft Design with Active Load Alleviation and Natural Laminar Flow," *53rd AIAA/ASME/ASCE/AHS/ASC Structures, Structural Dynamics and Materials Conference*, AIAA Paper 2012-1428, 2012.
<https://doi.org/10.2514/6.2012-1428>
- [3] Xu, J., and Kroo, I., "Aircraft Design with Active Load Alleviation and Natural Laminar Flow," *Journal of Aircraft*, Vol. 51, No. 5, 2014, pp. 1532–1545.
<https://doi.org/10.2514/1.C032402>
- [4] Heathcote, D. J., Gursul, I., and Cleaver, D. J., "Aerodynamic Load Alleviation Using Minitabs," *Journal of Aircraft*, Vol. 55, No. 5, 2018, pp. 2068–2077.
<https://doi.org/10.2514/1.C034574>
- [5] Cattafesta, L. N., and Sheplak, M., "Actuators for Active Flow Control," *Annual Review of Fluid Mechanics*, Vol. 43, No. 1, 2011, pp. 247–272.
<https://doi.org/10.1146/annurev-fluid-122109-160634>
- [6] Livne, E., "Aircraft Active Flutter Suppression: State of the Art and Technology Maturation Needs," *Journal of Aircraft*, Vol. 55, No. 1, 2018, pp. 410–452.
<https://doi.org/10.2514/1.C034442>
- [7] Liebeck, R. H., "Design of Subsonic Airfoils for High Lift," *Journal of Aircraft*, Vol. 15, No. 9, 1978, pp. 547–561.
<https://doi.org/10.2514/3.58406>
- [8] Gai, S. L., and Palfrey, R., "Influence of Trailing-Edge Flow Control on Airfoil Performance," *Journal of Aircraft*, Vol. 40, No. 2, 2003, pp. 332–337.
<https://doi.org/10.2514/2.3097>
- [9] Myose, R., Papadakis, M., and Heron, I., "Gurney Flap Experiments on Airfoils, Wings, and Reflection Plane Model," *Journal of Aircraft*, Vol. 35, No. 2, 1998, pp. 206–211.
<https://doi.org/10.2514/2.2309>
- [10] Date, J. C., and Turnock, S. R., "Computational Evaluation of the Periodic Performance of a NACA, 0012 Fitted with a Gurney Flap," *Journal of Fluids Engineering*, Vol. 124, No. 1, 2002, pp. 227–234.
<https://doi.org/10.1115/1.1427927>
- [11] Matalanis, C. G., Wake, B. E., Opoku, D., Min, B.-Y., Yeshala, N., and Sankar, L., "Aerodynamic Evaluation of Miniature Trailing-Edge Effectors for Active Rotor Control," *Journal of Aircraft*, Vol. 48, No. 3, 2011, pp. 995–1004.
<https://doi.org/10.2514/1.C031191>
- [12] Cooperman, A. M., Chow, R., and van Dam, C. P., "Active Load Control of a Wind Turbine Airfoil Using Microtabs," *Journal of Aircraft*, Vol. 50, No. 4, 2013, pp. 1150–1158.
<https://doi.org/10.2514/1.C032083>
- [13] Li, Y., Wang, J., and Zhang, P., "Influences of Mounting Angles and Locations on the Effects of Gurney Flaps," *Journal of Aircraft*, Vol. 40, No. 3, 2003, pp. 494–498.
<https://doi.org/10.2514/2.3144>
- [14] Wang, J., Li, Y., and Choi, K.-S., "Gurney Flap–Lift Enhancement, Mechanisms and Applications," *Progress in Aerospace Sciences*, Vol. 44, No. 1, 2008, pp. 22–47.
<https://doi.org/10.1016/j.paerosci.2007.10.001>
- [15] Heathcote, D. J., Gursul, I., and Cleaver, D., "An Experimental Study of Mini-Tabs for Aerodynamic Load Control," *54th AIAA Aerospace Sciences Meeting*, AIAA Paper 2016-0325, 2016.
<https://doi.org/10.2514/6.2016-0325>
- [16] Baker, J. P., Standish, K. J., and Van Dam, C. P., "Two-Dimensional Wind Tunnel and Computational Investigation of a Microtab Modified Airfoil," *Journal of Aircraft*, Vol. 44, No. 2, 2007, pp. 563–572.
<https://doi.org/10.2514/1.24502>
- [17] Bull, S., Chiereghin, N., Cleaver, D. J., and Gursul, I., "Novel Approach to Leading-Edge Vortex Suppression," *AIAA Journal*, Vol. 58, No. 10, 2020, pp. 4212–4227.
<https://doi.org/10.2514/1.J059444>
- [18] Hadjipantelis, M., Son, O., Wang, Z., and Gursul, I., "Frequency Response of Separated Flows on a Plunging Finite Wing with Spoilers," *Experiments in Fluids*, Vol. 65, No. 36, 2024, pp. 1–27.
<https://doi.org/10.1007/s00348-024-03775-3>
- [19] Lin, J. C., "Review of Research On Low-Profile Vortex Generators to Control Boundary-Layer Separation," *Progress in Aerospace Sciences*, Vol. 38, Nos. 4–5, 2002, pp. 389–420.
[https://doi.org/10.1016/S0376-0421\(02\)00010-6](https://doi.org/10.1016/S0376-0421(02)00010-6)
- [20] Taylor, H. D., "The Elimination of Diffuser Separation by Vortex Generators," United Aircraft Corp. Rept. R-4012-3, 1947.
- [21] Lin, J. C., "Control of Turbulent Boundary-Layer Separation Using Micro-Vortex Generators," *30th Fluid Dynamics Conference*, AIAA Paper 1999-3404, 1999.
<https://doi.org/10.2514/6.1999-3404>
- [22] "Vortex Generators for Control of Shock-Induced Separation. Part 2: Guide to Use of Vane Vortex Generators," ESDU-93025, 1995, https://www.esdu.com/cgi-bin/ps.pl?sess=unlicensed_1230510134034zrf&t=doc&p=esdu_93025a.
- [23] Tebbiche, H., and Boutoudj, M. S., "Vortex Generators Contribution to the Enhancement of the Aerodynamic Performances," *Advanced Materials Research*, Vol. 950, 2014, pp. 268–274.
<https://doi.org/10.4028/www.scientific.net/AMR.950.268>
- [24] Sørensen, N. N., Zahle, F., Bak, C., and Vronsky, T., "Prediction of the Effect of Vortex Generators on Airfoil Performance," *Journal of Physics: Conference Series*, Vol. 524, 2014, Paper 012019.
<https://doi.org/10.1088/1742-6596/524/1/012019>
- [25] Li, X.-K., Liu, W., Zhang, T.-J., Wang, P.-M., and W., X.-D., "Analysis of the Effect of Vortex Generator Spacing on Boundary Layer Flow Separation Control," *Applied Sciences*, Vol. 9, No. 24, 2019, p. 5495.
<https://doi.org/10.3390/app9245495>
- [26] Li, X.-K., Liu, W., Zhang, T.-J., Wang, P.-M., and Wang, X.-D., "Experimental and Numerical Analysis of the Effect of Vortex Generator Installation Angle on Flow Separation Control," *Energies*, Vol. 12, No. 23, 2019, p. 4583.
<https://doi.org/10.3390/en12234583>
- [27] Barrett, R., and Farokhi, S., "Subsonic Aerodynamics and Performance of a Smart Vortex Generator System," *Journal of Aircraft*, Vol. 33, No. 2, 1996, pp. 393–398.
<https://doi.org/10.2514/3.46950>
- [28] Quackenbush, T. R., McKillip, R. M., and Whitehouse, G. R., "Development and Testing of Deployable Vortex Generators Using SMA Actuation," *28th AIAA Applied Aerodynamics Conference*, AIAA Paper 2010-4686, 2010.
<https://doi.org/10.2514/6.2010-4686>
- [29] Calkins, F. T., Fassmann, A. W., Vijgen, P. M., Nicholson, D. E., Bass, M. A., and Benafan, O., "Shape Memory Alloy Actuated Vortex Generators: Shape Memory Alloy Reconfigurable Technology-Vortex Generators (Smart-VG) Can Reduce Fuel Consumption and Improve Aircraft Efficiency," *Advanced Materials & Processes*, Vol. 178, No. 3, 2020, pp. 60+.
- [30] Calkins, F. T., Nicholson, D. E., Fassman, A., Vijgen, P., Yeeles, C., and Benafan, O., "International Conference on Shape Memory and Superelastic Technologies," *SMST 2022: Extended Abstracts from the International Conference on Shape Memory and Superelastic Technologies*, 2022, pp. 6–8.
<https://doi.org/10.31399/asm.cp.smst2022p0006>

- [31] Cella, U., Quagliarella, D., Donelli, R., and Imperatore, B., "Design and Test of the UW-5006 Transonic Natural-Laminar-Flow Wing," *Journal of Aircraft*, Vol. 47, No. 3, 2010, pp. 783–795.
<https://doi.org/10.2514/1.40932>
- [32] Wild, J., *High-Lift Aerodynamics*, 1st ed., CRC Press, Boca Raton, FL, 2022.
- [33] Lock, R. C., "An Equivalence Law Relating Three-and Two-Dimensional Pressure Distributions," Aeronautical Research Council R&M 3346, 1962.
- [34] Anderson, J. D., *Introduction to Flight*, 5th ed., McGraw Hill, New York, 2005.
- [35] Xu, Z.-M., Han, Z.-H., and Son, W.-P., "An Improved 2.75D Method Relating Pressure Distributions of 2D Airfoils and 3D Wings," *Aerospace Science and Technology*, Vol. 128, 2022, Paper 107789.
<https://doi.org/10.1016/j.ast.2022.107789>
- [36] Streit, T., Wichmann, G., von Knoblauch zu Hatzbach, F., and Campbell, R. L., "Implications of Conical Flow for Laminar Wing Design and Analysis," *29th AIAA Applied Aerodynamics Conference*, AIAA Paper 2011-3808, 2011.
<https://doi.org/10.2514/6.2011-3808>
- [37] Menter, F. R., Sechner, R., and Matyushenko, A., *Best Practice: RANS Turbulence Modeling in Ansys CFD*, 1st ed., Ansys Inc., 2021.
- [38] Menter, F. R., "Zonal Two Equation k/Omega, Turbulence Models for Aerodynamic Flows," *AIAA Journal*, Vol. 32, No. 8, 1993, pp. 1993–2006.
<https://doi.org/10.2514/6.1993-2906>
- [39] Menter, F. R., "Two-Equation Eddy-Viscosity Turbulence Models for Engineering Applications," *AIAA Journal*, Vol. 32, No. 8, 1994, pp. 1598–1605.
<https://doi.org/10.2514/3.12149>
- [40] Cook, P. H., McDonald, M. A., and Firmin, M. C. P., "Aerofoil RAE 2822—Pressure Distributions, and Boundary Layer and Wake Measurements Experimental Data Base for Computer Program Assessment," AGARD TR AR 138, 1979.
- [41] Slater, J., "NPARC Alliance Validation Archive—RAE 2822 Transonic Airfoil: Study 1," 1998, <https://www.grc.nasa.gov/WWW/wind/valid/raetaf/raetaf01/raetaf01.html>.
- [42] RAE2822 Airfoil—Validation, DAfoamDocumentation, 2024, https://dafoam.github.io/mydoc_validations_rae2822.html.

B. Glaz
Associate Editor